IOP Conf. Series: Materials Science and Engineering **84** (2015) 012079 doi:10.1088/1757-899X/84/1/012079

Synchrotron X-ray Tomographic Quantification of Deformation Induced Strain Localisation in Semi-solid Al-15wt.%Cu

B. Cai[1], S. Karagadde[1], T.J. Marrow[2], T. Connolley[3], P.D. Lee[1]

1 School of Materials, University of Manchester, Manchester, UK
2 Department of Materials, University of Oxford, Oxford, UK
3 Diamond Light Source Ltd., Harwell Science and Innovation Campus, Didcot, UK

Email: peter.lee@manchester.ac.uk

Abstract Uniaxial compression and indentation of a semi-solid Al-15wt.%Cu alloy was investigated by high speed synchrotron X-ray microtomography, quantifying the microstructural response of a solidifying alloy to applied strain. Tomograms were continuously acquired whilst performing deformation using a precision thermal-mechanical rig on a synchrotron beamline. The results illustrate how defects and shear bands can form in response to different loading conditions. Using digital volume correlation, the global and localised strains were measured, providing quantitative datasets for granular flow models of semi-solid deformation.

1. Introduction

Semi-solid processing (SSP) is being considered over conventional casting processes for some aerospace and automotive components, as it is thought to give improved mechanical properties. However, defects are still known to occur [1]. Many of the early studies, such as that by Spencer et al [2], looked at the shear-thinning behaviour in semi-solid Sn-Pb. Since that time, numerous studies have been conducted to determine the constitutive properties of partially solidifying alloys using deformation methods such as rotation viscometer, compression, and indentation. The authors of these studies have proposed a range of behaviours, ranging from shear-thinning (thixotropic) [2], shear-thickening [3], and treatment as a continuum 'spongy-like' solid network saturated with liquid [4]. However, these prior studies did not link material behaviour to the detailed kinetics occurring at the microstructural scale during deformation, in which there is a complex interaction of evolving solid and liquid in a solidifying alloy.

One method of overcoming this limitation of linking defect formation to microstructure was demonstrated by Lee and Hunt [5] who developed an X-ray Temperature Gradient Stage for performing in situ radiographic observations of defect formation. Recent years have seen the development of X-ray in situ observation by various groups to study semi-solid deformation, both via radiography [6–8] and tomography [9–12]. Gourlay and co-workers [7,13] designed a direct shear cell to use in situ radiography to study granular deformation in a semi-solid. Cai et al [12] and Kareh et al [14] used parallel plate compression together with high speed synchrotron X-ray microtomography (XMT) to investigate the occurrence of dilatancy in semi-solid dendritic and globular microstructures, respectively. An extrusion cell was also coupled with high speed XMT to investigate deformation-

induced flow in a semi-solid alloy [11]. In addition to performing qualitative in situ observations of deformation-induced microstructural changes, there is a need to quantify the strain localization induced by deformation in semi-solids. This has been made possible by advanced image processing methods, for example, strain fields have been measured in 2D via a particle tracking technique [13] and in 3D using digital volume correlation (DVC) [12].

In this study, we quantify material flow at a microstructural level in 3D in semi-solid equiaxed dendritic structures for uniaxial compression and indentation tests. This was achieved using high speed synchrotron X-ray tomography combined with digital volume correlation, allowing a quantitative investigation of deformation induced strain localization and failure mechanisms.

2. Materials and Methods

An equiaxed dendritic Al-15wt%Cu alloy with a grain size of ~600 μm was used. Semi-solid deformation tests (both compression and indentation) were carried out using the bespoke P2R thermo-mechanical rig, with air-bearing continuous rotation built into the load chain [12]. The experiments were performed at the I12 beamline, Diamond Light Source, with a monochromatic, 53 keV X-ray beam. X-ray imaging was performed using the beamline's custom-built imaging modules, consisting of single crystal scintillators lens-coupled to a CMOS high speed camera.

For the compression test, a Phantom V7.3 CMOS camera (Vision Research, USA) was used, providing a field of view (FOV) of 800×600 pixels (9.8 ×7.3 mm) and a pixel size of 12.25 μm. The cylindrical sample (3 mm in diameter and 4 mm height) was heated in the furnace to 555°C (liquid fraction of 30±2%), and held isothermally for 10 min during which slight coarsening occurred. The sample was then compressed at a displacement rate of 5 μm/s. After deforming for 20 s, high speed X-ray tomographic imaging was started, and 24 datasets were captured over 96 s (i.e. one tomogram every 4 s, each 720 projections collected over 180° rotation).

For the indentation test, a Miro 310M CMOS camera (Vision Research, USA) was used, offering 1280×800 pixels (5.12×3.2 mm) FOV and 4 μm pixel size. A cylindrical (3 mm in diameter and 3 mm height) sample was used. The 30° conical indenter was made of alumina. The sample was heated to 555 °C with liquid fraction of 28% and held for 10 min. The deformation was then started at a speed of 5 μm/s. Continuous scans were taken at an interval of 18 s, acquiring 900 projections in 9 s over 180°. Nine datasets were captured in total.

All captured datasets were reconstructed with a filtered back projection algorithm, including ring artefact removal [15]. 3D image visualization was performed using Avizo 8 (Visualization Science Group, France). DaVis Strain Master (Version 8.0.7, LaVision, GmBH, Germany) was used to perform digital volume correlation (DVC) on the time-resolved 3D datasets, providing a full-field displacement field and 3D strain map [12,16,17]. The samples used in this study have a complex dendritic structure providing the texture required for DVC tracking via contrast between the α-Al primary phase and Cu-rich interdendritic liquid. The compression datasets were analysed by a final 24 × 24 × 24 pixel subset with 50% overlap. Hence a displacement matrix grid of 12 pixels or 147 μm was obtained. The indentation datasets were analysed using 64 × 64 × 64 interrogation subsets with 50% overlap, offering a 32 pixel displacement matrix (128 μm). Displacement vectors with a correlation coefficient less than 0.5 were deleted. Figure 1 schematically illustrates the application of digital volume correlation for the determination of the strain field on the time-revolved X-ray tomographic datasets. The displacement fields (V_m, m = 1, 2, 3⋯) were calculated from the nearby tomographic dataset (step 1→step 2, step 2→step 3⋯). Then the measured displacements were accumulated (i, i+ii, i+ii+iii …) to calculate the integrated displacement fields (V_n (n = I, II, III…)) in the data series. The integrated displacement fields were used to calculate the strain tensor ($\square_j$ ($i, j = x, y, z$) by the finite difference method.

$$\varepsilon_{ij} = \frac{\partial V_i}{\partial j}$$

The strain tensor was then used to calculate three principal strain components. The first component of the principal strain (ε_1) is used to demonstrate the strain field.

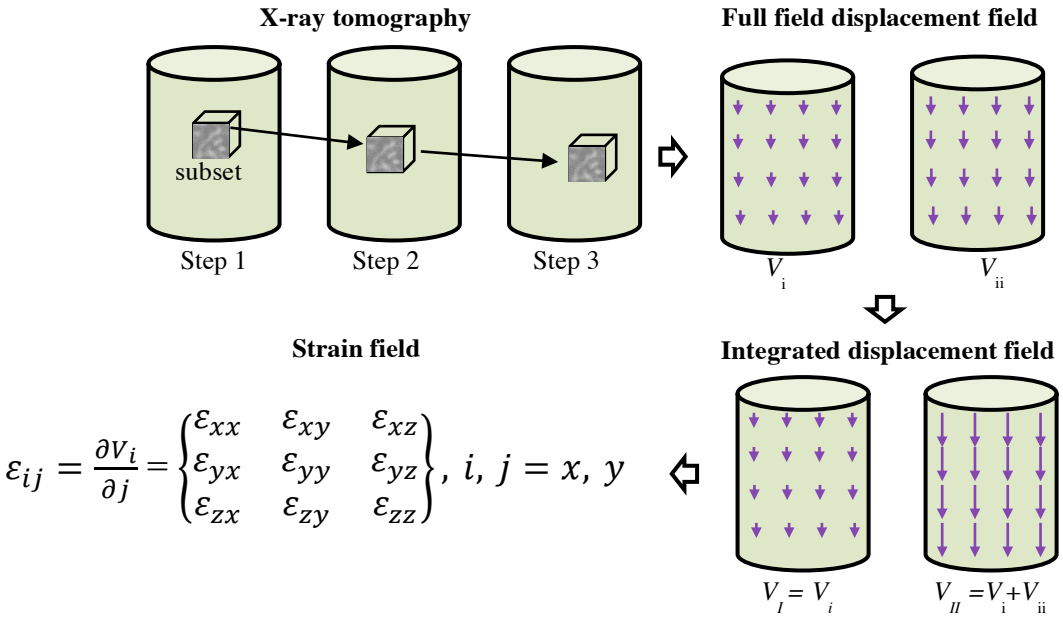

Figure 1. Schematic of the full-field strain measurement using digital volume correlation on time-revolved X-ray tomographic datasets

3. Results and Discussion

3.1. Semi-solid compression

Parallel plate compression is one of the standard methods of measuring the properties of solid materials, and it has also been used to determine the rheology properties of semi-solid alloys. In this study, a semi-solid Al15wt%Cu specimen (liquid fraction of 30%) was compressed at 5 μm/s. The results are shown in Fig. 2 for four sequential steps, with the solid coloured red and the liquid yellow. The initial microstructure consists of equiaxed-dendritic grains with homogeneously distributed Cu-enriched interdendritic liquid surrounding them (Fig. 2a).

As compression proceeds, the sample becomes slightly barrelled (Fig. 2b, ε = 4.8% as measured tomographically by the change of sample height). The barrelling is due to the friction between the platens (made of pyrophyllite) and the semi-solid sample. It can be seen that the liquid channel opened slightly at the middle region of the sample with liquid flowing into the opening. As compression continues, the liquid channels enlarge (Fig. 2c, ε = 7.3% and 2d, ε = 12.6%), due to dilatancy. Voids nucleate at the periphery of the sample (Fig. 2b & 2c), growing along the liquid channels and penetrating all the way into the centre of the sample (Fig. 2d). These results support the three stage growth of voids hypothesised in [12]: (1) initial void closure, (2) incubation and (3) final rapid growth.

This increase in liquid-filled interstices and the initiation of voids during semi-solid compression is due to dilatancy, as discovered by Reynolds in 1885 for granular solids [18]. Several studies have confirmed the role of dilatancy in semi-solid alloys. Tzimas and Zavaliangos [19] reported the occurrence of dilatancy in semi-solid equiaxed alloys during compression. Gourlay et al [20] used a rotation viscometer and revealed that partially solidified alloys can exhibit Reynolds' dilatancy. Recently, dilatancy has also been imaged by X-ray radiographic experiments [21]. Our study demonstrates that dilatancy in the semi-solid alloys was caused by the rearrangement of grains responding to the applied deformation. As the grains translate and rotate, the gaps between them increase, and interdendritic liquid first fills the dilated interstices. When liquid is no longer able to feed the increased dilation, gas is drawn in from the edges to form voids along dilated liquid channels.

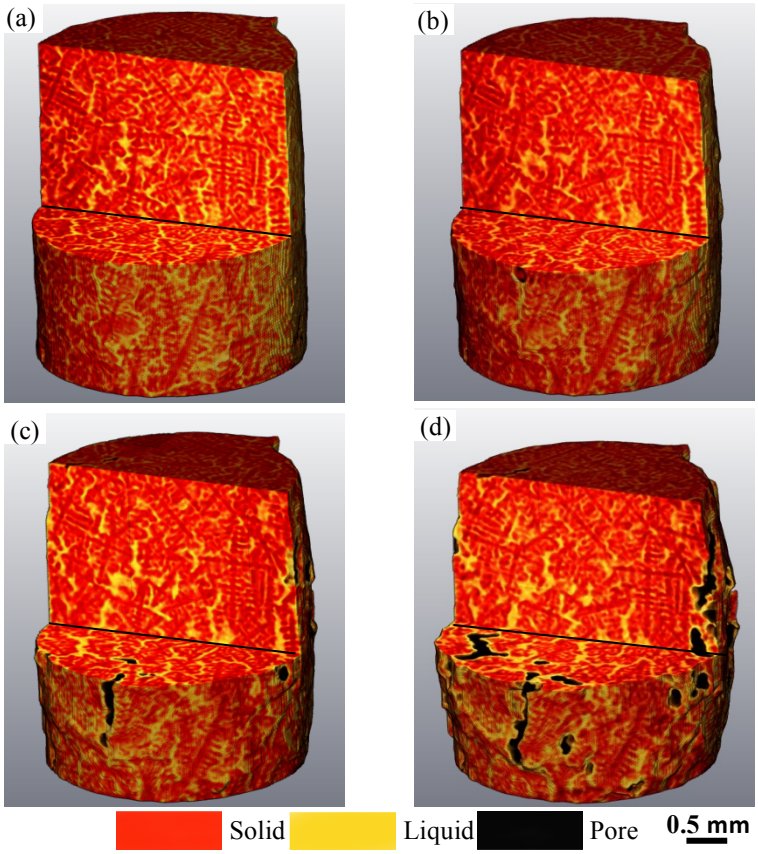

Figure 2. X-ray tomograms of semi-solid Al-15 wt.%Cu alloy (fraction liquid of 30 ± 2%) at four stages of compression: (a) t = 24 s, ε = 1.2%; (b) t = 52 s, ε = 4.8 %, (c) t = 76 s, ε = 7.3%; and (d) t = 116 s, ε = 12.6%

The distribution of the principal strain (ε_1) as measured by DVC is shown on the outer surface and cross-section of the specimen in Fig. 3, at four stages of compression. The iso-surface of ε_1 equal to 20% is rendered in red in the other half of the specimen, showing the localisation of the strain into shear bands. The highest strain levels are first observed in the regions where the interdendritic channels widen between grains, followed by subsequent void / damage formation, often connected to the surface of the sample (compare Figs. 2d & 3d). Once voids form, there is no texture for DVC tracking. Hence, a cylindrical mask of 2.7 mm diameter was used to cut out those regions. Nevertheless, Fig. 3 reveals the extent of strain localisation during semi-solid compression. Going through the successive compression steps, initially the strain is homogeneous (Fig. 3a, axial strain 3.6%). However, when compressed to ε = 7.3%, localisation starts to occur as the grains contact, rotating and shearing (Fig. 3b), although ε_1 larger than 20% is still negligible. When compressed to ε = 10.2% (Fig. 3c), dilatant effects become even stronger, and there is a considerable increase of the fraction of ε_1 larger than 20% with the on-set of what appears to be shear banding. At the final stage of deformation (ε = 12.6%), ε_1 is connected to the edge of the cylindrical mask, with strong bands of localised strain (Fig. 3d). The inhomogeneity of strain distribution during semi-solid compression is directly related to the deformation response at the grain scale: (1) the movement and interplay of solid grains causing contact and rotation of the primary alpha phase grains, as well as (2) bending and fragmentation of the dendritic structures [12].

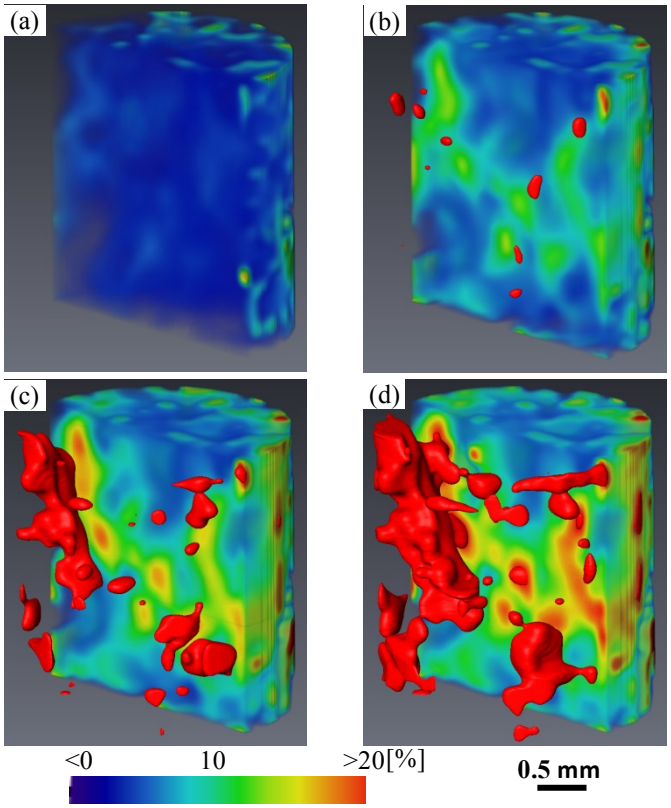

Figure 3. 3D rendering of the first principal strain during semi-solid compression (red iso-surface represents ε_1=20%) at axial strains of: (a) 3.6%; (b) 7.3%; (c) 10.2%; and (d) 12.6%

3.2. Semi-solid indentation

In the second example we investigate the behaviour of semi-solid (fraction liquid 30%) Al-15wt.%Cu during indentation. Indentation is a standard method of measuring the hardness and other properties of solids, but little has been published on the behaviour of semi-solids during this type of deformation [19]. Indentation has been demonstrated to produce highly localized deformation in the vicinity of the indenter in highly ductile alloys even at room temperature [11], providing an interesting comparison to the aforementioned uniaxial compression.

Figure 4 shows results of indenting a semi-solid at an indenter displacement rate of 5 μm/s at four indentation penetration depths. The equiaxed dendritic microstructure of the initial sample when held isothermally at 555±2 °C is clearly visible in Fig. 4a. After only 90 μm of indentation, the highly localised strain around the indenter is visible by the localised opening of liquid channels. The localised contact of the indenter on the grains pushed the grains downwards and sideways, whereas the liquid channels and grain locations far below the indenter appear unaffected. Applying the force with an indenter causes the dilatant behaviour to be highly localised, much like walking on wet sand causes dilatant expansion of the sand only where you stepped, leaving dry footprints behind.

As the indenter travels deeper into the sample, the force chains expand downwards and sideways to the periphery of the sample (Fig. 4c), with liquid channels opening up all the way to the edges. In Fig. 4d the liquid channel on the right hand side of indenter increases (black arrow), whilst the just-opened liquid channel on the left hand side (blue arrow in Fig. 4c) closes. In addition, the secondary dendrites within the equiaxed grain directly below the indenter compact. This shows the interplay of dilatant effects and deformation of the solid phase, with both plastic strain and granular flow occurring.

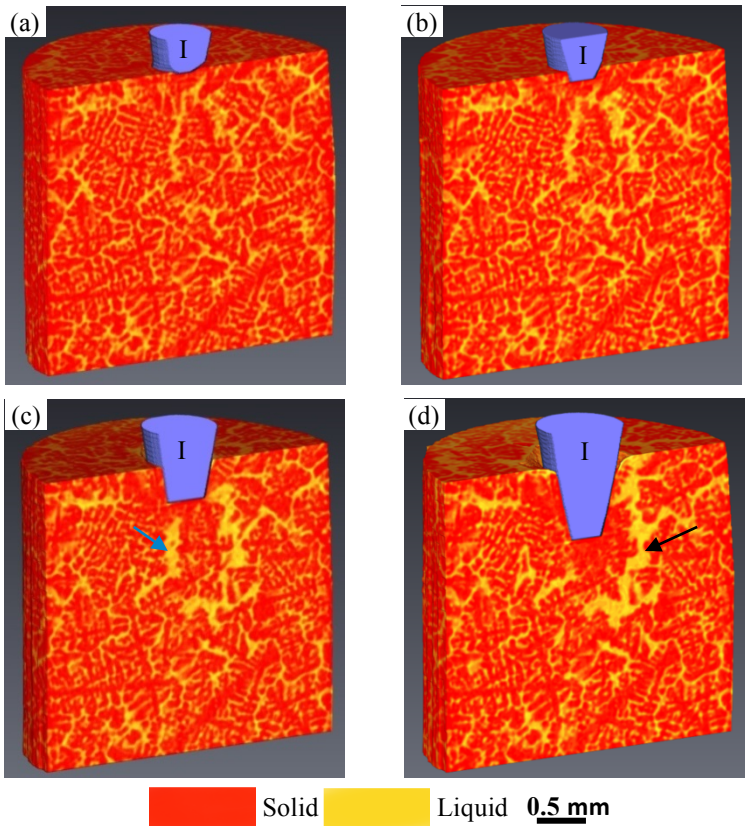

Figure 4. Semi-solid Al-15wt%Cu at subsequent stages of indentation: (a) $t = 0$ s, I = 0 μm; (b) $t = 18$ s, I = 90 μm; (c) $t = 54$ s, I = 270 μm; (d) $t = 126$ s, I = 630 μm

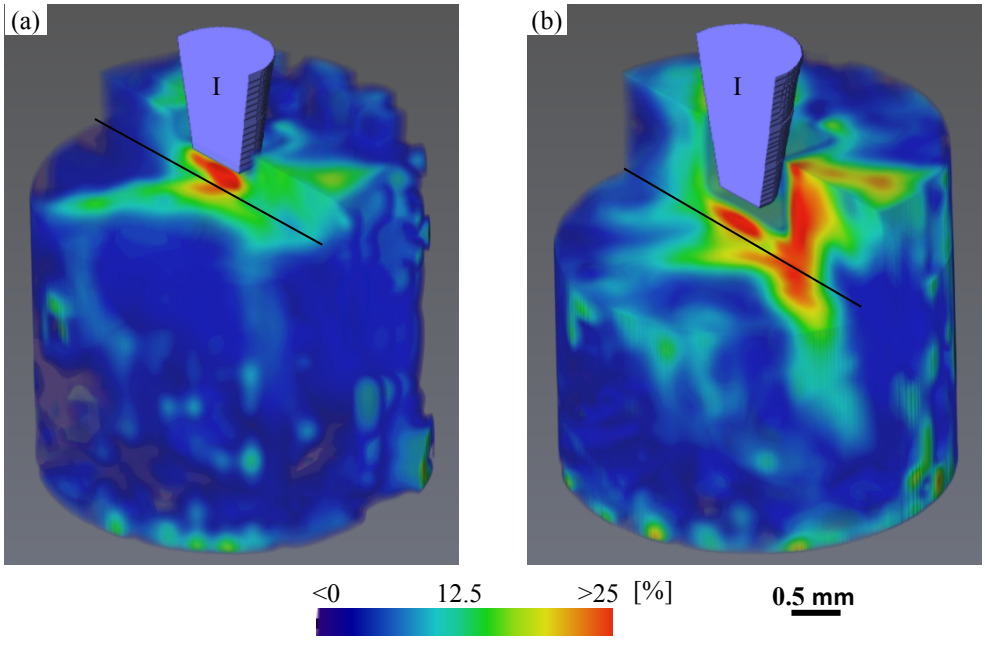

Figure 5. First principal strain in semi-solid Al-15wt%Cu at indenter locations of: (a) 360 µm, (b) 630 µm

The principal strain (ε_1) field is shown at two stages of indentation in Fig. 5, as calculated using digital volume correlation. The distribution of ε_1 at 360 μm indentation is shown in Fig. 5a, with the majority of the strain localised directly below the indenter. As the indenter presses further into the sample (630 μm, Fig. 5b) the principal strain increases further. However, ε_1 now rises not only beneath the indenter, as the grains contact one onto the next, the force chains and strain extend all the way to the sides and bottom of the sample, but in a very heterogeneous manner.

4. Conclusions

The use of in situ X-ray tomography combined with digital volume correlation has allowed the formation of strain localisation and defect formation to be quantitatively studied during two typed of deformation of an Al15wt.%Cu alloy (semi-solid compression and indentation). The results demonstrate that equiaxed dendritic semi-solids behave in both a granular flow regime (exhibiting strong dilatancy), and also undergo plastic deformation. These experiments show the role of microstructure upon the relative importance of these different types of deformation, depending on both the way the deformation is applied, and the overall strain. This data can serve as both the input geometries and validation for models of microstructural deformation during solidification and semi-solid processing.

Acknowledgements

This work was financially supported by the EPSRC (EP/I02249X/1) and the European Union (RFSR-PR-10005 DDT). We thank Diamond Light Source for providing beamtimes (experimental visits EE7604-1 and EE9018-1), and Dr. Robert Atwood at beamline I12 for his help. We are grateful to Vision Research UK for the loan of the Miro 310M camera. B.C. acknowledges financial support from General Electric and the China Scholarship Council.

References

[1] Atkinson H. Prog Mater Sci 2005;50:341.
[2] Spencer DB, Mehrabian R, Flemings MC. Metall Trans A 1972;3:1972.
[3] Kumar P, Martin CL, Brown S. Metall Trans A 1993;24:1107.
[4] Nguyen TG, Favier D, Suéry M. Int J Plast 1994;10:663.
[5] Lee PD, Hunt JD. Acta Mater 1997;45:4155.
[6] Phillion AB, Hamilton RW, Fuloria D, Leung ACL, Rockett P, Connolley T, Lee PD. Acta Mater 2011;59:1436.
[7] Gourlay CM, Dahle AK, Nagira T, Nakatsuka N, Nogita K, Uesugi K, Yasuda H. Acta Mater 2011;59:4933.
[8] Zabler S, Ershov A, Rack A, Garcia-Moreno F, Baumbach T, Banhart J. Acta Mater 2013;61:1244.
[9] Terzi S, Salvo L, Suéry M, Limodin N, Adrien J, Maire E, Pannier Y, Bornert M, Bernard D, Felberbaum M. Scr Mater 2009;61:449.
[10] Puncreobutr C, Lee PD, Hamilton RW, Cai B, Connolley T. Metall Mater Trans A 2012;44:5389.
[11] Cai B, Karagadde S, Rowley D, Marrow TJ, Connolley T, Lee PD. Scr Mater 2015.
[12] Cai B, Karagadde S, Yuan L, Marrow TJ, Connolley T, Lee PD. Acta Mater 2014;76:371.
[13] Nagira T, Morita S, Yokota H, Yasuda H, Gourlay CM, Yoshiya M, Sugiyama A, Uesugi K, Takeuchi A, Suzuki Y. Metall Mater Trans A 2014;45:5613.
[14] Kareh KM, Lee PD, Atwood RC, Connolley T, Gourlay CM. Nat Commun 2014;5:4464.
[15] Titarenko S, Withers PJ, Yagola A. Appl Math Lett 2010;23:1489.
[16] Mostafavi M, Collins DM, Cai B, Bradley R, Atwood RC, Reinhard C, Jiang X, Galano M, Lee PD, Marrow TJ. Acta Mater 2015;82:468.
[17] Eastwood DS, Yufit V, Gelb J, Gu A, Bradley RS, Harris SJ, Brett DJL, Brandon NP, Lee PD, Withers PJ, Shearing PR. Adv Energy Mater 2014;4:1.

[18] Reynolds O. Philos Mag J Sci 1885;20:470.
[19] Tzimas E, Zavaliangos A. Acta Mater 1999;47:517.
[20] Gourlay CM, Dahle A. Nature 2007;445:70.
[21] Gourlay CM, Nagira T, Dahle AK, Nakatsuka N, Uesugi K, Yasuda H. IOP Conf Ser Mater Sci Eng 2012;27:012086.